Institutional Repository - Research Portal
Dépôt Institutionnel - Portail de la Recherche
researchportal.unamur.be
University of Namur

RESEARCH OUTPUTS / RÉSULTATS DE RECHERCHE

A cytoplasmic chemoreceptor and reactive oxygen species mediate bacterial chemotaxis to copper

Louis, Gwennaëlle; Cherry, Pauline; Michaux, Catherine; Rahuel-Clermont, Sophie; Dieu, Marc; Tilquin, Françoise; Maertens, Laurens; Van Houdt, Rob; Renard, Patricia; Perpete, Eric; Matroule, Jean Yves

Published in:
Journal of Biological Chemistry

DOI:
10.1016/j.jbc.2023.105207

Publication date:
2023

Document Version
Publisher's PDF, also known as Version of record

Link to publication

Citation for pulished version (HARVARD):
Louis, G, Cherry, P, Michaux, C, Rahuel-Clermont, S, Dieu, M, Tilquin, F, Maertens, L, Van Houdt, R, Renard, P, Perpete, E & Matroule, JY 2023, 'A cytoplasmic chemoreceptor and reactive oxygen species mediate bacterial chemotaxis to copper', *Journal of Biological Chemistry*, vol. 299, no. 10, 105207. https://doi.org/10.1016/j.jbc.2023.105207

General rights
Copyright and moral rights for the publications made accessible in the public portal are retained by the authors and/or other copyright owners and it is a condition of accessing publications that users recognise and abide by the legal requirements associated with these rights.

- Users may download and print one copy of any publication from the public portal for the purpose of private study or research.
- You may not further distribute the material or use it for any profit-making activity or commercial gain
- You may freely distribute the URL identifying the publication in the public portal ?

Take down policy
If you believe that this document breaches copyright please contact us providing details, and we will remove access to the work immediately and investigate your claim.

Download date: 27. Apr. 2024

JBC RESEARCH ARTICLE

A cytoplasmic chemoreceptor and reactive oxygen species mediate bacterial chemotaxis to copper

Received for publication, March 10, 2023, and in revised form, August 16, 2023 Published, Papers in Press, September 1, 2023,
https://doi.org/10.1016/j.jbc.2023.105207

Gwennaëlle Louis[1], Pauline Cherry[1], Catherine Michaux[2], Sophie Rahuel-Clermont[3], Marc Dieu[4], Françoise Tilquin[1], Laurens Maertens[1,5], Rob Van Houdt[5], Patricia Renard[4], Eric Perpete[2], and Jean-Yves Matroule[1,*]

From the [1]Research Unit in Biology of Microorganisms (URBM), Department of Biology, Namur Research Institute for Life Sciences (NARILIS), and [2]Laboratoire de Chimie Physique des Biomolécules, Namur Research Institute for Life Sciences (NARILIS) and Namur Institute of Structured Matter (NISM), University of Namur, Namur, Belgium; [3]CNRS, IMoPA, Université de Lorraine, Nancy, France; [4]MaSUN, Mass Spectrometry Facility, University of Namur, Namur, Belgium; [5]Microbiology Unit, Interdisciplinary Biosciences, Belgian Nuclear Research Centre (SCK CEN), Mol, Belgium

Reviewed by members of the JBC Editorial Board. Edited by Ursula Jakob

Chemotaxis is a widespread strategy used by unicellular and multicellular living organisms to maintain their fitness in stressful environments. We previously showed that bacteria can trigger a negative chemotactic response to a copper (Cu)-rich environment. Cu ion toxicity on bacterial cell physiology has been mainly linked to mismetallation events and reactive oxygen species (ROS) production, although the precise role of Cu-generated ROS remains largely debated. Here, using inductively coupled plasma optical emission spectrometry on cell fractionates, we found that the cytoplasmic Cu ion content mirrors variations of the extracellular Cu ion concentration. ROS-sensitive fluorescent probe and biosensor allowed us to show that the increase of cytoplasmic Cu ion content triggers a dose-dependent oxidative stress, which can be abrogated by superoxide dismutase and catalase overexpression. The inhibition of ROS production in the cytoplasm not only improves bacterial growth but also impedes Cu chemotaxis, indicating that ROS derived from cytoplasmic Cu ions mediate the control of bacterial chemotaxis to Cu. We also identified the Cu chemoreceptor McpR, which binds Cu ions with low affinity, suggesting a labile interaction. In addition, we demonstrate that the cysteine 75 and histidine 99 within the McpR sensor domain are key residues in Cu chemotaxis and Cu coordination. Finally, we discovered that *in vitro* both Cu(I) and Cu(II) ions modulate McpR conformation in a distinct manner. Overall, our study provides mechanistic insights on a redox-based control of Cu chemotaxis, indicating that the cellular redox status can play a key role in bacterial chemotaxis.

Cell motility is widely distributed across the three domains of life. For instance, in animals, it is involved in fertilization, and in neutrophils recruitment to an inflammatory area. It also allows archaea and bacteria to seek nutrients in scarce environments and to flee from toxic compounds while it supports to some extent host tropism in the frame of symbiotic relationships.

Most of the time, cell motility is driven by chemical gradients and is therefore named chemotaxis. In flagellated bacteria, positive (attraction) and negative (repulsion) chemotactic responses imply stochastic direction changes triggered by the inversion of flagellar rotation (1, 2). This switch is caused by the binding of the phosphorylated response regulator, CheY∼P, to the flagellar motor. Spontaneous or phosphatase-mediated CheY∼P dephosphorylation by the CheZ phosphatase or by a member of the CheC/CheX/FliY phosphatase family triggers CheY release from the flagellar motor (3–5). The release of CheY promotes a straight bacterial swimming pattern until CheY is phosphorylated again and triggers a new direction change. CheY phosphorylation relies on the histidine kinase CheA, which is recruited and autophosphorylated within a chemotaxis cluster composed of cytoplasmic or inner membrane–spanning methyl-accepting chemotaxis proteins (Mcp), also named chemoreceptors (6). Chemoreceptors are classically composed of an N-terminal sensing domain, transmembrane (TM) domains (which are absent in cytoplasmic chemoreceptors), a HAMP domain, and the C-terminal (Mcp) signaling domain. Depending on their cellular topology, chemoreceptors monitor chemical variations in the cytosol or in the periplasm *via* their N-terminal sensing domain. Upon substrate binding to their sensing domain, chemoreceptors undergo a conformational change leading to the increase (repellent response) or the decrease (attractant response) of CheA histidine kinase activity (7, 8). In *Escherichia coli* Tar and Tsr chemoreceptors, this conformational change consists in a 2 Å shift of one of the TM helices (TM2), causing a "piston-like" movement in the direction of the membrane that impacts the HAMP domain (9). The methylation of the Mcps by the CheR methyltransferase results in an increase of CheA activity, and their demethylation by the CheA-activated CheB methylesterase leads to the decrease of CheA activity (9). This adaptation response sets back the Mcps in a prestimulus state.

Copper (Cu) has been used for centuries as an antimicrobial and antifouling strategy in medicine and in various

* For correspondence: Jean-Yves Matroule, jean-yves.matroule@unamur.be.

© 2023 THE AUTHORS. Published by Elsevier Inc on behalf of American Society for Biochemistry and Molecular Biology. This is an open access article under the CC BY license (http://creativecommons.org/licenses/by/4.0/).

anthropogenic activities including agriculture and industry. Cu toxicity in solution mainly results from its high redox potential causing the displacement of native metallic ions from metalloproteins and the disruption of Fe–S clusters (10). Cu ability to generate reactive oxygen species (ROS) has been shown *in vitro* (11), but the role of these ROS *in vivo* yet remains unclear. In a previous study, we identified an original bimodal strategy to cope with Cu stress where the flagellated morphotype (swarmer [SW] cell) of *Caulobacter crescentus* triggers a prompt negative chemotaxis from the Cu source (12). In addition to the negative Cu chemotaxis, *C. crescentus* exhibits a positive chemotactic behavior toward xylose (13) and O_2 (14), but no dedicated Mcp could be identified so far.

C. crescentus genome harbors two chemotaxis operons. The major chemotaxis operon encodes McpA and McpB, CheYI and CheYII, CheAI, one CheW, CheRI, CheBI, and the CheY-like CleA. This operon also contains the *cheD*, *cheU*, and *cheE* genes, which have been hardly described. CheYII and CheBI are likely the major CheY and CheB in *C. crescentus* chemotaxis (15, 16). The alternate chemotaxis operon encodes McpG and McpK, two CheY, CheAII, one CheW, CheBII, and CheRII. The other *cheY* genes and the third *cheW* are dispersed within the genome. Only the first chemotaxis operon seems to be essential for chemotaxis, whereas both operons are involved in biofilm formation and holdfast production, by regulating the expression of the *hfiA* holdfast inhibitor (16, 17).

No CheZ homolog has been found in *C. crescentus* genome, but the multiple CheY homologs are proposed to act as phosphate sinks to allow the termination process, such as in *Rhizobium meliloti* (18). Five of the CheY have been redefined as Cle proteins (CheY-like c-di-GMP effectors) and renamed CleA to CleE. CleA and CleD could compete with CheYII to prevent the rotational switch of the flagellum and to promote straight run (15). The *C. crescentus* Mcp array exhibits a higher-ordered hexagonal structure constituted of approximatively 1000 to 2000 Mcps per array (19). Among the *C. crescentus* Mcps, only the inner membrane McpA and the cytoplasmic McpB encoded by the major chemotaxis operon were described as polar chemoreceptors, although their exact function remains unknown (20).

In the present study, we aimed to decipher the sensing mechanism underlying *C. crescentus* chemotaxis to a toxic Cu-rich environment. We provide evidence that an increased intracellular Cu concentration triggers a dose-dependent production of ROS, which is a prerequisite to Cu chemotaxis. We also demonstrate that the redox status of the Cu ions bound to the sensor domain of the newly identified McpR modulates McpR conformation *in vitro*. This original redox sensing mechanism may ensure a continuous monitoring of the intracellular Cu status, providing a real-time control of the chemotactic response.

Results

To further dissect the molecular mechanisms underlying the negative Cu chemotaxis of *C. crescentus* SW cells (12), we first sought to identify the chemoreceptor involved in Cu chemotaxis. The genome of *C. crescentus* is predicted to encode 19 chemoreceptors (named McpA to McpS) based on the presence of an Mcp domain binding CheA/CheW (21). No canonical Cu ion–binding site, including the CXXC motif or the βαββαβ fold (22), could be found by running manual and JPred4-based analyses of the 19 chemoreceptor protein sequences (23). Therefore, we proceeded to single in-frame deletions of the 19 *mcp* genes, and their respective chemotactic behavior to Cu ions was assessed by using the previously designed live chemotaxis imaging (LCI) (12). Most of the Δ*mcp* mutants displayed a WT-like behavior with a flight percentage after 25 min varying between 15% and 51%. Only Δ*mcpA*, Δ*mcpB*, and Δ*mcpR* mutants showed a significant decrease of Cu chemotaxis relative to the WT strain (Fig. 1*A*), suggesting that these chemoreceptors might be involved in Cu chemotaxis. The Δ*mcpA*, Δ*mcpB*, and Δ*mcpR* mutants could be complemented by the expression of an ectopic version of *mcpA*, *mcpB*, and *mcpR* on a low copy plasmid, respectively, ruling out any polar effect of the deletions (Fig. S1). Owing to the position of the *mcpA* gene within the major chemotaxis cluster (16), McpA is likely involved in chemotaxis to a less specific extent. Consistent with this hypothesis, the Δ*mcpA* mutant displays a reduced motility halo in a Cu ion–free swarming assay, whereas the Δ*mcpB* and Δ*mcpR* mutants exhibit a WT-like chemotaxis profile in the same condition (Fig. S2*A*). The presence of the terminal sequence of the CheB/CheR docking site in McpB (absent from McpR) led us to the idea that McpB might be necessary for the adaptive response as in *E. coli* (24), which will not be considered in this study. Therefore, we decided to determine how McpR modulates Cu chemotaxis.

The ability of the Δ*mcpR* mutant to form a motility halo in a Cu ion–free swarming assay (Fig. S2*A*) and to sustain negative chemotaxis to other chemicals, such as zinc (Zn) ions (Fig. S2*B*), indicates that the loss of Cu chemotaxis in the Δ*mcpR* mutant does not result from a loss of motility and/or a disruption of the general chemotactic machinery.

McpR harbors the canonical domain organization found in chemoreceptors including an N-terminal sensing domain followed by a HAMP domain and a C-terminal Mcp domain. McpR sequence analysis using the TMHMM 2.0 (DTU Health Tech) (25) and SignalIP 6.0 (DTU Health Tech) (26) tools did not reveal any McpR TM domain and signal peptide, respectively, arguing for a cytoplasmic localization for McpR, and therefore a sensing of the cytoplasmic Cu content.

Chemoreceptors can sense attractants or repellents in a direct manner or an indirect manner *via* their sensing domain (27). The 3D structure prediction of McpR by Alphafold2 (28, 29) highlights a cysteine (C75) in the vicinity of a histidine (H99) in the McpR sensing domain (Fig. 1*B*). Cysteine and histidine residues have often been described as key residues in Cu coordination (30), suggesting that McpR may bind Cu ions directly.

Therefore, we used intrinsic fluorescence spectroscopy to assess the direct binding of Cu to the purified McpR. Upon the addition of either Cu(I) ions or Cu(II) ions, the intrinsic McpR fluorescence at 346 nm is quenched in a dose-dependent

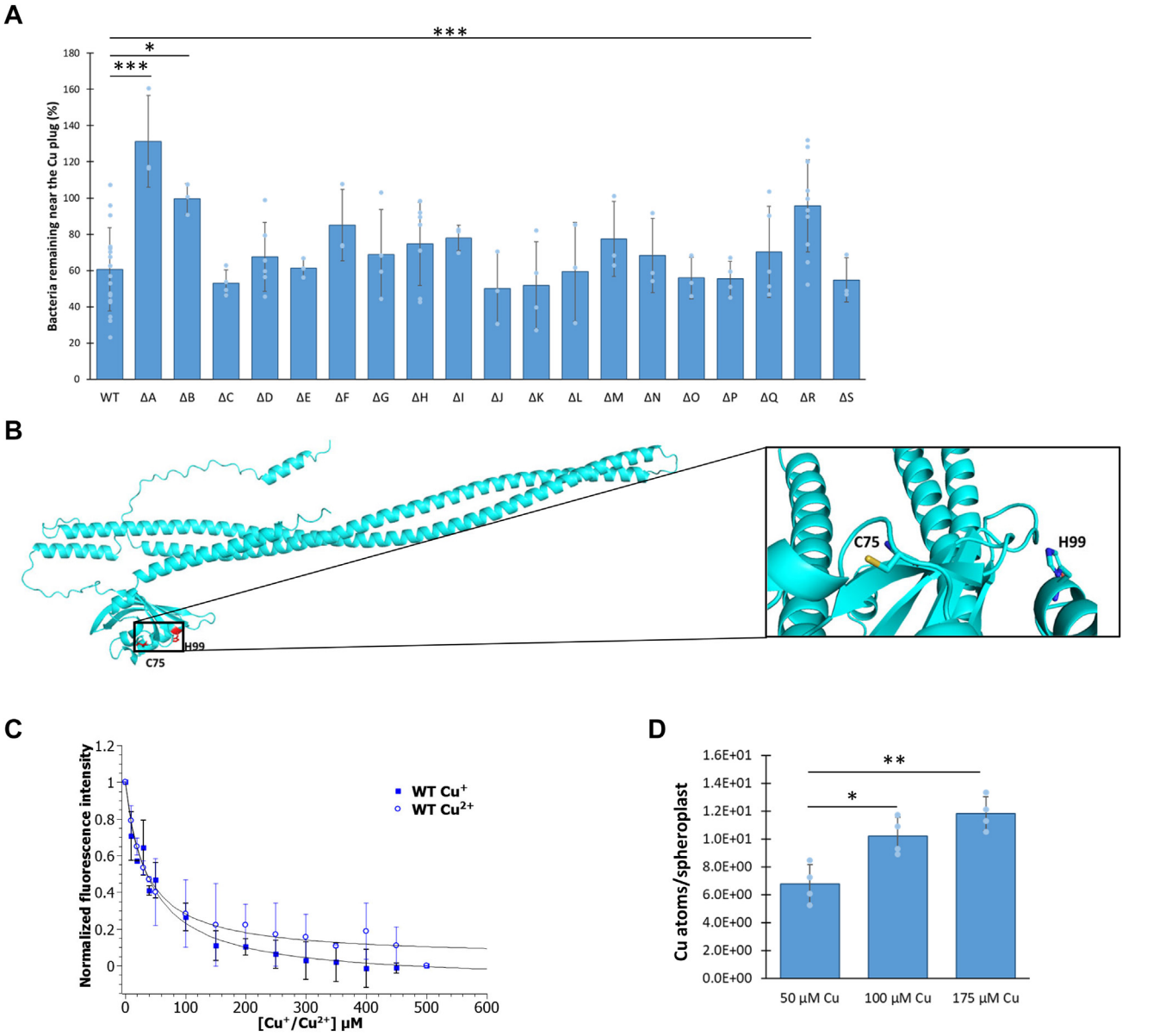

Figure 1. McpR is involved in Cu chemotaxis and Cu binding. *A*, percentage of WT and Δ*mcp* (*mcpA* to *mcpS*) SW cells remaining in the vicinity of the Cu plug after 25 min. *B*, 3D structure prediction of McpR by AlphaFold. H99 and C75 residues are highlighted. *C*, McpR titration by Cu(I) (*full squares*) or Cu(II) (*circles*) monitored by protein intrinsic fluorescence intensity quenching, fitted to a single-site hyperbolic model by nonlinear regression analysis (*solid line*). The fluorescence intensity changes are normalized to the maximum fluorescence intensity change. *D*, number of Cu atoms per spheroplast from SW cells exposed to various Cu concentrations for 5 min. Mean ± SD, at least three biological replicates. *p* Values were calculated using an ANOVA (*$p < 0.05$, **$p < 0.01$, and ***$p < 0.001$) (Table S1). Cu, copper; SW, swarmer cell.

manner, reflecting a modification of the McpR aromatic residue environment (Fig. 1*C*). The dissociation constants (K_d) (see Experimental procedures section for calculation method) of 48 µM ± 10 µM for Cu(I) ions and 37 µM ± 9 µM for Cu(II) ions attest to a similar affinity of both ionic forms for McpR. However, the micromolar range of Cu(I) ion and Cu(II) ion K_ds exceeds from several logs the K_d of well-known cuproproteins (31, 32), arguing for a rather labile interaction between McpR and Cu. Nevertheless, McpR seems to preferentially bind Cu ions since Zn, cadmium (Cd), manganese, and nickel ions had no effect on purified McpR intrinsic fluorescence (Fig. S3).

To determine whether the cytoplasmic Cu ion content could reflect variations of the extracellular Cu ion concentration when the SW cell swims away from a Cu ion source, we measured by inductively coupled plasma optical emission spectrometry (ICP-OES) the Cu ion content in cytoplasmic fractions from SW cells subjected to increasing Cu ion concentrations. Although the measurement cannot discriminate between free and complexed Cu ions, Cu(I) and Cu(II), we measured a dose-dependent accumulation of Cu ions in the cytoplasm (Fig. 1*D*). This observation is in accordance with previous data from our laboratory, showing that an artificial decrease of Cu ion content *via* the overexpression of the PcoB

efflux pump impeded Cu chemotaxis (12). Together, these data suggest that the sensing of cytoplasmic Cu ions by McpR could be used as a proxy by the SW cells to mirror variations of the concentration of Cu ions in *C. crescentus* environment to control Cu chemotaxis.

The transient maintenance of a high intracellular Cu ion content in the SW cells may potentially lead to an oxidative stress *via* the production of superoxide anion ($O_2^{\bullet-}$), hydrogen peroxide (H_2O_2), and hydroxyl radical ($OH^{\bullet}$) (Fig. S4*A*). In line with this idea, the relative fluorescence intensity of the ROS-sensitive turn-on CellROX Deep Red (ThermoFisher) probe is significantly increased in SW cells exposed to Cu ions, and H_2O_2, the latter being used as a positive control (Fig. 2*A*). Accordingly, the fluorescence of the cytoplasmic turn-off rxYFP redox biosensor is partially quenched under the same conditions (Fig. 2*B*), mirroring an imbalance of the cytoplasmic GSH–GSSG pool upon oxidative stress (Fig. S4*B*). These findings are reinforced by the differential expression of genes involved in oxidative stress response upon Cu stress, including those encoding the catalase KatG and the superoxide dismutases SodA and SodB (33). As observed for the cytoplasmic Cu ion content (Fig. 1*D*), the amount of ROS is increased when the SW cells are exposed to increasing extracellular Cu ion concentrations, indicating that the cytoplasmic ROS level mirrors the cytoplasmic Cu ion content (Fig. 2*C*).

We envisioned that boosting the antioxidant defense system would limit ROS production by Cu ions. Therefore, we ectopically expressed the *sodB* gene or the *katG* gene in the WT background from a low copy plasmid under the control of the strong and constitutive *lac* promoter. The resulting *sodB*$^+$ and *katG*$^+$ strains prevent the increase of the CellROX Deep Red fluorescence upon SW cell exposure to Cu ions, reflecting a potentiation of antioxidant defenses (Fig. 2*D*). In support of these data, the growth of these two optimized *sodB*$^+$ and *katG*$^+$ strains is improved under moderate Cu stress (Fig. 2*E*), arguing for a role of $O_2^{\bullet-}$ and H_2O_2 in Cu toxicity.

Interestingly, the *sodB*$^+$ and *katG*$^+$ strains are impeded in Cu chemotaxis similarly to the Δ*cheAI* mutant (Fig. 2*F*, SI Appendix, and Fig. S5), indicating that the ROS resulting from the accumulation of cellular Cu ions play a role in Cu chemotaxis. It is worth mentioning that the loss of Cu chemotaxis in the Δ*mcpR* mutant is not because of a loss of ROS production under Cu stress since the Δ*mcpR* mutant exhibits a similar decrease of the rxYFP fluorescence to the WT strain upon Cu ion exposure (Fig. S6). These data support a major role of the ROS resulting from Cu ion accumulation in Cu chemotaxis and indicate that Cu ions binding to McpR are solely not sufficient to sustain Cu chemotaxis.

An LC–MS analysis of McpR revealed a significant oxidation of the McpR sensor domain (residues 1–161) and more specifically of the H99 residue when purified McpR is incubated *in vitro* with Cu(I) ions + H_2O_2 and with Cu(I) ions, although at a lower extent (Fig. 3*A*, *left panel*). In Cu(I) ions + H_2O_2 condition, about 30% of the H99 residues acquired an additional oxygen atom, most likely yielding 2-oxoHis. Metal ion–catalyzed oxidation of histidines *via* the generation of $OH^{\bullet}$ has been previously described in the *Bacillus subtilis* PerR repressor (34), yeast SOD1 (35), and amyloid beta peptide (36). The exact role of this modification remains unknown, and no redox cycling involving 2-oxoHis has been described so far, questioning the relevance of H99 oxidation in Cu/ROS sensing. Metal ion–catalyzed oxidation mostly targets the metal-binding residues in a caged process (37), reinforcing the Cu binding to McpR (Fig. 1*C*) and suggesting that H99 may coordinate Cu. To test this hypothesis, we purified an $McpR_{H99A}$ mutant protein and calculated the K_d values of the $McpR_{H99A}$/Cu(I) ion and $McpR_{H99A}$/Cu(II) ion complexes (Figs. 3*B* and S7*A* for the *fitting curves*). H99A mutation triggers a 9.4- and 5.8-fold increase of Cu(I) ion and Cu(II) ion K_ds, respectively, relative to McpR, suggesting a key role of H99 in Cu(I) ion and Cu(II) ion coordination. The important variability associated with the $McpR_{H99A}$ K_d values likely reflects a potential instability of this mutant in solution upon Cu(I) ion and Cu(II) ion exposure, resulting in the presence of several subpopulations of $McpR_{H99A}$.

The protocol used for the LC–MS analysis performed on McpR *in vitro* did not allow us to monitor the metal-catalyzed oxidation of the neighboring C75 residue as observed for the H99 residue. To assess the potential implication of the C75 residue in Cu ion coordination, we purified the $McpR_{C75S}$ mutant protein and calculated the K_d values of the $McpR_{C75S}$/Cu(I) ion and $McpR_{C75S}$/Cu(II) ion complexes. As for the H99A mutation, the C75S mutation also impeded Cu(I) ion binding as attested by a 3.5-fold K_d increase. Cu(II) ion binding to the $McpR_{C75S}$ mutant remained unchanged (Figs. 3*B* and S7*B* for the *fitting curves*), suggesting that McpR C75 is required to coordinate Cu(I) ions but not Cu(II) ions. Consistent with this observation, *in vitro* H99 oxidation by Cu(I) ions $\pm H_2O_2$ is fully abolished in the $McpR_{C75S}$ variant (Fig. 3*A*, *right panel*). The K_d values calculated for the $McpR_{C75S}$ and $McpR_{H99A}$ variants are in agreement with the known selective binding of Cu(I) and Cu(II) ions to cysteine and histidine residues (30, 38).

To determine whether Cu coordination by McpR H99 and C75 residues is essential to Cu chemotaxis, we decided to express an ectopic $mcpR_{H99A}$ allele or $mcpR_{C75S}$ allele in the Δ*mcpR* mutant and to monitor the chemotactic behavior of both strains to Cu ions. None of the mutant allele was able to complement the Cu-chemotaxis defect of the Δ*mcpR* mutant (Fig. 3*C*). One could argue that the $McpR_{H99A}$ and $McpR_{C75S}$ variants are unstable *in vivo*, explaining the Δ*mcpR* mutant phenotype. In accordance with the pleiotropic sensing ability of some Mcps, we discovered that McpR is also playing a key role in Cd chemotaxis (Fig. S8). Interestingly, the $mcpR_{H99A}$ and $mcpR_{C75S}$ mutant strains were not impeded in Cd chemotaxis (Fig. S8). This latter observation attests the integrity of the $McpR_{H99A}$ and $McpR_{C75S}$ variants *in vivo* and suggests that Cd sensing by McpR does not rely on the H99 and C75 residues.

These data led us to the idea that Cu(I) ion coordination by McpR H99 and C75 residues is decisive for McpR-mediated Cu chemotaxis. Given the structural changes elicited by the

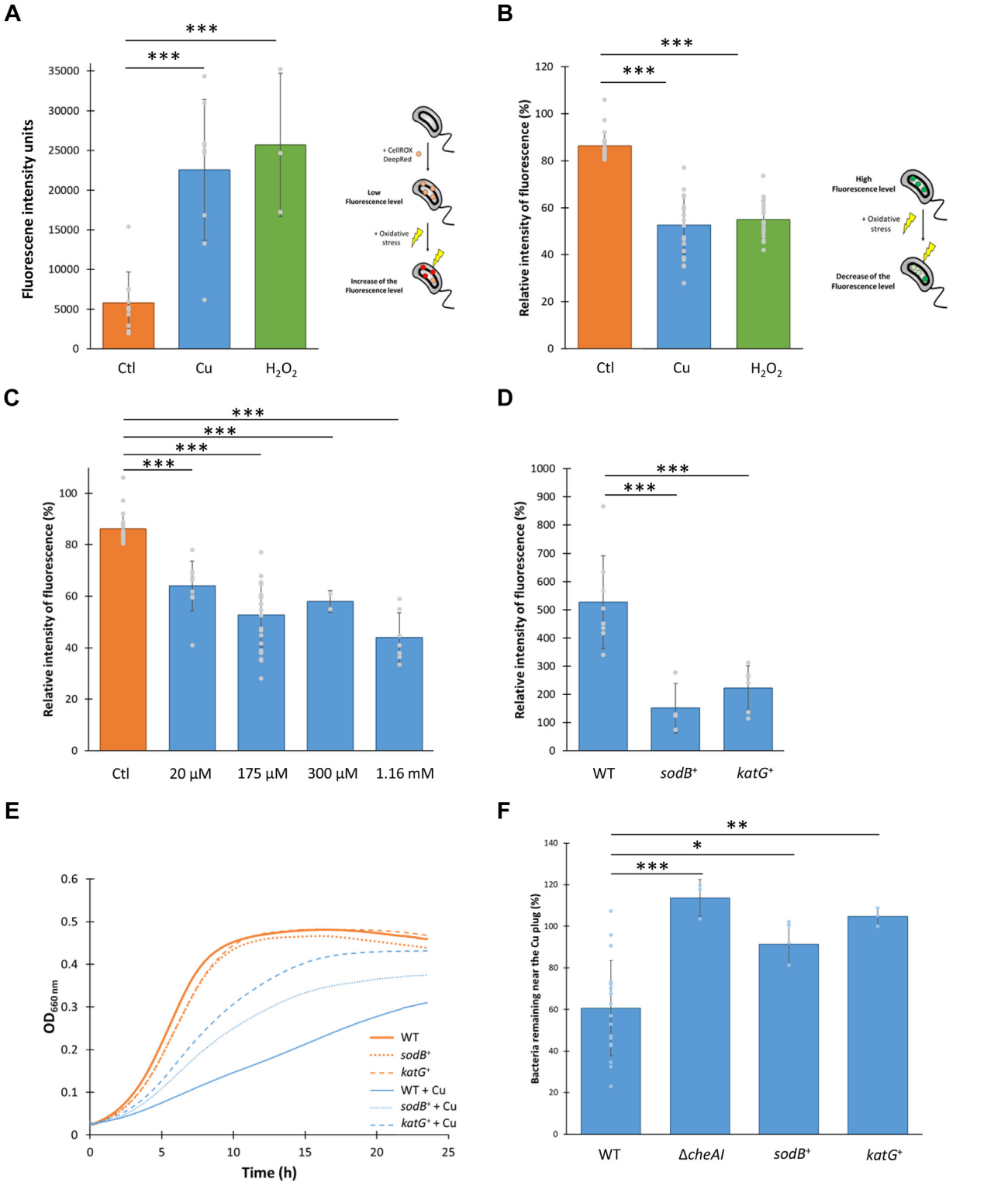

Figure 2. Cu-induced ROS sustain Cu chemotaxis. *A*, raw fluorescence of SW cells incubated with 5 µM CellROX Deep Red probe and exposed to 175 µM Cu or 400 µM H_2O_2. *B*, relative fluorescence intensity of SW cells expressing the rxYFP biosensor and exposed to 175 µM Cu or 400 µM H_2O_2 for 20 min. *C*, relative fluorescence intensity of SW cells expressing the rxYFP biosensor and exposed to various Cu concentrations for 20 min. *D*, relative fluorescence intensity of WT SW cells and SW cells overexpressing SodB (*sodB*+) and KatG (*katG*+) incubated with 5 µM CellROX Deep Red probe and exposed to 175 µM Cu. *E*, growth profiles at an absorbance at 660 nm of WT, *sodB*+, and *katG*+ strains in PYE (*orange*) and exposed to 175 µM Cu (*blue*). *F*, percentage of WT, Δ*cheAI*, *sodB*+, and *katG*+ SW cells in the vicinity of the Cu plug after 25 min. Mean ± SD, at least three biological replicates, except for 300 µM Cu (two biological replicates). *p* Values were calculated using an ANOVA when appropriate (*$p < 0.05$, **$p < 0.01$, and ***$p < 0.001$) (Table S1). Cu, copper; PYE, peptone yeast extract; ROS, reactive oxygen species; SW, swarmer cell.

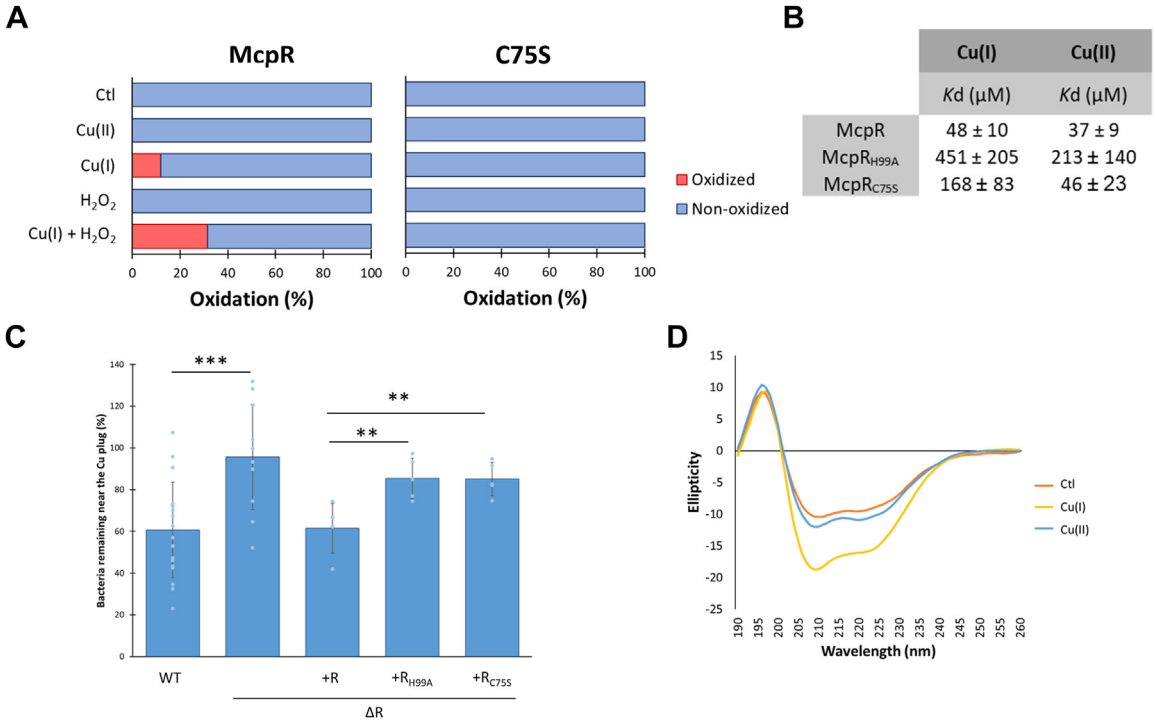

Figure 3. Cu cycling modulates its coordination by McpR. *A*, percentage of oxidation of the H99 residue from purified McpR (*left panel*) and McpRC75S (*right panel*) incubated with Cu(II), Cu(I), H_2O_2, and Cu(I) + H_2O_2 at a 1:100 ratio. *B*, measure, by intrinsic fluorescence, of the K_d values of purified McpR, McpRH99A, and McpRC75S (1.79 μM) incubated with 0 to 500 μM Cu(I) and Cu(II). Mean ± SD. *C*, percentage of WT, Δ*mcpR*, and Δ*mcpR* overexpressing McpR, McpRH99A, or McpRC75S SW cells remaining in the vicinity of the Cu plug after 25 min. Mean ± SD, at least three biological replicates. *p* Values were calculated using an ANOVA (*$p < 0.05$, **$p < 0.01$, and ***$p < 0.001$) (Table S1). *D*, CD spectra of purified McpR (8.95 μM) incubated with Cu(I) and Cu(II) at a 1:100 ratio. Cu, copper.

binding of a ligand to a cognate chemoreceptor (39), we envisioned that Cu(I) ions binding to McpR could modulate its conformation. To test this idea, far-UV CD spectroscopy was used to monitor the impact of Cu(I) ions and Cu(II) ions on McpR secondary structure *in vitro*. Accordingly, Cu(I) ions has a more significant impact than Cu(II) ions on McpR secondary structure (Fig. 3*D*), increasing the α-helix percentage from 23% to 44%.

Based on our findings, we propose that Cu exposure triggers a dose-dependent Cu accumulation within the cytoplasm triggering a dose-dependent production of ROS that will sustain Cu chemotaxis. The increase in cytoplasmic Cu ion concentration will likely favor a rather labile Cu ion binding to the McpR sensor domain. Cu(I) ion coordination by McpR C75 and H99 residues triggers McpR conformational change. Interestingly, Cu(II) ions seem to preferentially bind McpR H99 residue and does not modify the apo form-like conformation. These observations suggest that a redox cycling of the McpR-bound Cu atom could modulate McpR conformation (Fig. 4).

Discussion

The role of ROS in Cu toxicity and Cu stress response remains largely unknown in bacteria. We sought to address this gap in the frame of negative chemotaxis to toxic Cu in the dimorphic bacterial model *C. crescentus*.

Our study identified the first Cu sensing chemoreceptor hereafter named McpR. McpR is devoid of any TM domains or signal peptide and is therefore predicted to localize in the cytoplasm. Cytoplasmic chemoreceptors have been shown to monitor the cellular metabolic state (40), whereas inner membrane chemoreceptors usually sense the periplasmic environment, as a proxy for extracellular changes. The cytoplasmic Cu content varies in a dose-dependent manner when the SW cells are exposed to Cu, suggesting that the sensing of cytoplasmic Cu could provide a sensitive monitoring of subtle variations of Cu concentrations when the SW cell swims down a Cu gradient.

In a previous study, we showed that the maintenance of a high cellular Cu concentration is critical for Cu chemotaxis (12). Consistent with this observation, we provide evidence that McpR binds Cu with low affinity. Although aspecific Cu binding to noncognate residues cannot be ruled out, the significant difference in K_d values measured between the WT McpR and the $McpR_{H99A}$ and $McpR_{C75S}$ variants argues for a Cu binding to these residues. Considering that Cu binding to McpR is a prerequisite for Cu chemotaxis, one could propose that when the SW cell is sufficiently far from the Cu source, the resulting low cytoplasmic Cu content impedes Cu binding to McpR and in turn the chemotactic response.

We also demonstrate that the cellular Cu accumulation triggers a dose-dependent production of ROS. This dose dependency in ROS production argues that the increase of extracellular Cu ion content triggers an increase of the cytoplasmic Cu ion labile pool, which is likely involved in the labile Cu binding to McpR. ROS production can be prevented by the

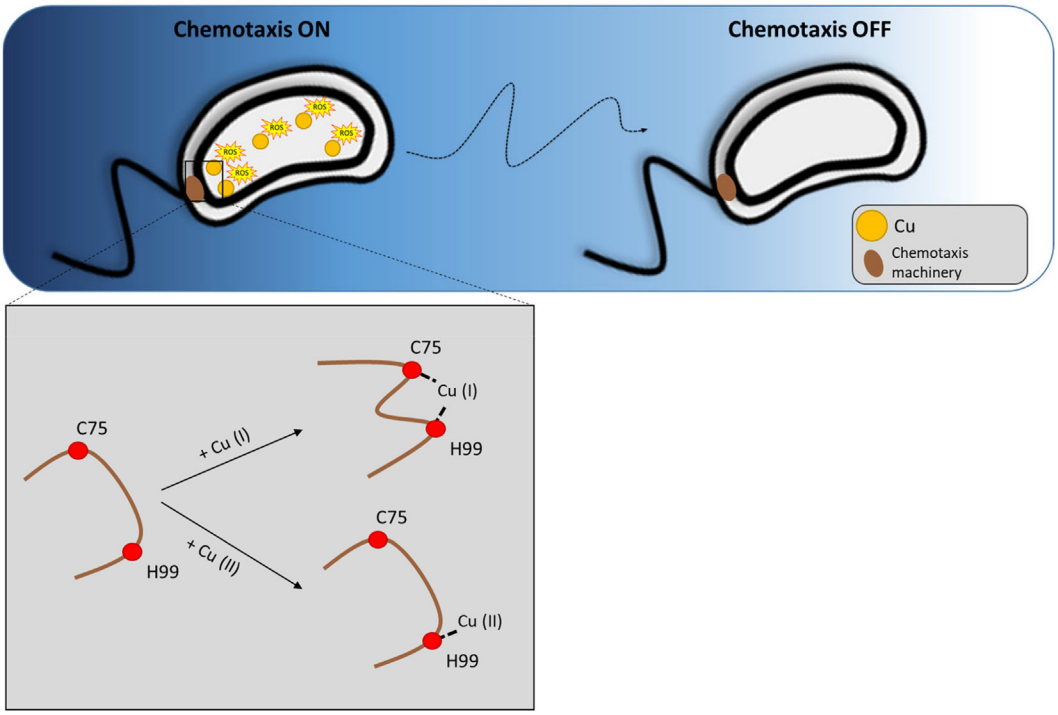

Figure 4. Hypothetical model of Cu sensing by McpR. SW cell exposure to Cu increases the cytoplasmic Cu concentration, leading to the generation of ROS (*left*). In addition, high cytoplasmic Cu content favors Cu(I) coordination by the C75 and H99 residues within the cytoplasmic McpR, triggering a conformational change of the chemoreceptor. Cu(II) binding to H99 residue has no impact on McpR apo-like conformation, suggesting a redox-dependent modulation of McpR conformation. This process would be maintained along the extracellular Cu gradient until the SW cell reaches a Cu-poor environment (*right*). Under these conditions, the cytoplasmic Cu concentration together with the ROS level would return to their basal level, and the labile Cu binding to McpR would be hindered, bringing McpR to its apo form conformation. Cu, copper; ROS, reactive oxygen species; SW, swarmer cell.

overexpression of SodB superoxide dismutase and KatG catalase, suggesting that at least $O_2^{\bullet-}$ and H_2O_2 are generated under Cu stress. The contribution of the ROS derived from cellular Cu ions in Cu toxicity is still largely debated (41, 42). Here, we demonstrate that ROS derived from cellular Cu ions not only impede cell growth to some extent but also play a key role in Cu chemotaxis. The exact target of ROS in Cu chemotaxis was not identified in this study, but one could hypothesize that $O_2^{\bullet-}$ is rapidly converted into H_2O_2. The latter would feed a local Fenton-like reaction catalyzed by the Cu(I) atom coordinated by McpR C75 and McpR H99 residues. This would lead to a local $OH^{\cdot}$ production and to the oxidation of McpR-bound Cu(I) into McpR-bound Cu(II). Owing to the reducing cytoplasmic environment, McpR-bound Cu(II) could in turn be reduced by cytoplasmic electron donors such as GSH, NADH, and thioredoxin to restore the Cu(I) ionic form. Thereby, the McpR-bound Cu ion would undergo a redox cycling involving the Cu(I) and Cu(II) ionic forms, which would be maintained as long as H_2O_2 is produced by cytoplasmic Cu ions. Cu-generated ROS would therefore act as second messengers in a bacterial stress response.

The modulation of the CheA–CheY two-component system results from a conformational change of the chemoreceptor occurring upon ligand binding (9). We demonstrated here that McpR conformation is modulated by the ionic status of the Cu atom bound to McpR. It should be emphasized that chemoreceptors are usually organized in trimers of dimers and assembled in large arrays in cells (43). Therefore, it is possible that Cu coordination by the McpR C75 and H99 residues within the McpR array implies two McpR monomers from one or two distinct dimers. Nevertheless, McpR conformational change likely regulates the downstream effectors such as CheAI and the resulting chemotactic response.

The diversity of chemoreceptors produced by a single bacterial species varies from 5 to 60 chemoreceptors and is often correlated to its lifestyle (40). Nevertheless, chemoreceptors are not always specific to one single substrate and can also perform indirect sensing *via* a substrate transporter (27). For instance, the *E. coli* Tar chemoreceptor directly senses aspartate and performs an indirect sensing of maltose through a periplasmic maltose-binding protein (44).

The extrapolation of our findings to other motile bacterial species based on sequence analyses is complicated by (i) the large diversity of Cu coordination mechanisms and thereby the low predictability of Cu-binding sites by *in silico* analyses and (ii) the low conservation of the Mcp sensor domains. Nevertheless, it is very likely that the use of ROS as second messengers is widely conserved in bacterial response to Cu.

Experimental procedures

Bacterial strains, plasmids, and growth conditions

C. crescentus (NA1000 strain) was grown at 30 °C in peptone yeast extract (PYE) medium (45) with 5 μg/ml kanamycin, 1 μg/ml chloramphenicol, and/or an appropriate concentration of

$CuSO_4.5H_2O$ when required. Cultures in exponential phase were used for all experiments. Strains, plasmids, and primers used in this study are listed in Table S2, and the strategies for their construction are available upon request. SW cell isolation was achieved accordingly (46). Briefly, the bacteria were collected at an absorbance of 0.4 at 660 nm and centrifuged in Ludox LS colloidal silica gradient. After the centrifugation, SW cells are separated from the other cellular forms (ST and PD) based on a density difference. The SW cells were collected and washed several times with PBS prior to the experiments.

Growth curve measurements

C. crescentus exponential phase cultures were diluted in PYE medium to a final absorbance of 0.05 at 660 nm and inoculated in 96-well plates with appropriate $CuSO_4$ concentration when required. Bacteria were then grown for 24 h at 30 °C under continuous shaking in an Epoch 2 Microplate Spectrophotometer from BioTek. The absorbance at 660 nm was measured every 10 min.

Motility assay

C. crescentus cultures grown in PYE were diluted to an absorbance of 0.4 at 660 nm and inoculated with sterile toothpicks on a PYE swarming plate (PYE + 0.25% agar). The plates were incubated at 30 °C for 3 days and then imaged.

Determination of cytoplasmic Cu content

C. crescentus cells were fixed for 20 min in 2% paraformaldehyde at 4 °C and then washed three times with an ice-cold wash buffer (10 mM Tris–HCl [pH 6.8] and 100 μM EDTA). The cells were then incubated for 10 min with zwitterionic detergent (0.0125% Zwittergent 3-14 detergent and 200 mM Tris–HCl [pH 7.6]) to disrupt the outer membrane but not the inner membrane. A final centrifugation at 14,500*g* for 15 min separated the spheroplasts (cytoplasm and inner membrane fraction) from the periplasm (and outer membrane fraction). The spheroplasts were lysed under 2.4 kbar by using a cell disrupter (Cell Disruption System, one shot model, Constant). Cell debris were removed by centrifugation at 10,000*g* for 10 min, and cell lysates were diluted in 1% HNO_3. Samples were finally analyzed by ICP-OES with an Optima 8000 ICP-OES from PerkinElmer. Cellular Cu concentrations were calculated as described (12). Briefly, 10 μl of the samples after fixation were diluted 1:100 in PBS and counted with a BD FACSVerse flow cytometer. Data were analyzed with the BD FACSuite V1.0.5 software. A ratio between the number of bacteria and the absorbance at 660 nm was determined. The combination of both flow cytometry and ICP-OES analyses allows to determine the number of Cu atoms in one spheroplast. Cu concentration was calculated using the following formula;

$$\frac{\frac{Amount\ of\ Cu\ (mg)}{Molecular\ weight\ of\ Cu\ \left(63{,}546\frac{mg}{L}\right)} \times Avogadro\ constant\ (6.022 \times 10^{23})}{Number\ of\ bacteria}$$

Oxidative stress measurement with the CellROX Deep Red probe

An exponential phase culture of *C. crescentus* was synchronized to isolate the SW cells. The isolated SW cells were diluted to a final absorbance of 0.2 at 660 nm and incubated for 30 min at 30 °C under moderate shaking with 5 μM of CellROX Deep Red probe and appropriate concentrations of $CuSO_4$ or H_2O_2. The bacteria were then washed three times with 20 mM phosphate buffer (12.5 mM Na_2HPO_4, 8 mM KH_2PO_4, pH 7) to remove the non-internalized probe. The bacteria were finally transferred into a black bottom 96-well plate, and the fluorescence was monitored at emission/excitation of 640/690 nm with a SpectraMax iD3 (Molecular Devices). The relative fluorescence intensity was determined by defining 100% as the fluorescence from control condition.

Oxidative stress measurement with the rxYFP biosensor

The SW cells were synchronized from an exponential phase culture overexpressing the rxYFP biosensor (47). The SW cells were diluted to a final absorbance of 0.4 at 660 nm in a black bottom 96-well plate and mixed with different concentrations of $CuSO_4$ and H_2O_2. The rxYFP fluorescence was then monitored every minute for 20 min at emission/excitation of 510/556 nm with a SpectraMax iD3. The relative fluorescence intensity was determined by defining 100% as the initial measured fluorescence at time 0.

LCI

The LCI assay was adapted from Ref. (12). Briefly, chemotaxis devices were made by casting solubilized 10:1 polydimethylsiloxane (PDMS Slygard 184; Dow Corning) in a small glass pot (d = 50 mm; h = 30 mm; glassware from Lenz laborglass instrument) in which coverslips were initially installed to mold the future bacterial chamber. The PDMS was left overnight, allowing degassing and curing. The different channels were drilled into the PDMS devices. A microscope slide and the PDMS cube were washed successively with acetone (only the slide), isopropanol, methanol, and rinsed with Milli-Q H_2O. The materials were blown dry between each wash. The PDMS cube was sealed to the slide by pressure. Eight microliters of melted 1.5% agarose H_2O with appropriate concentration of $CuSO_4$, $ZnSO_4$, or $CdSO_4$ were loaded into the chamber through the external inlet channels to generate the plug. About 150 μl of isolated SW cells were in turn injected into the bacterial chamber through the central inlet channel. Images were collected every minute for 25 min in one focal plan (near the liquid surface) in the vicinity of the plug with a Nikon Eclipse Ti2-E inverted microscope equipped with a Nikon 20×/0.5 Ph2 objective and with a Hamamatsu C13440 digital camera. Quantitative analysis of the time-lapse images was performed with MicrobeJ, an ImageJ plug-in (48). The number of bacteria in a same focal plane was determined at each time point; the number of bacteria at the beginning of the experiment is considered as 100%.

ASBMB

Protein expression and purification

A BL21 pET28a-$McpR_{His}$ exponential phase culture was incubated for 3 h under shacking at 37 °C with 1 mM IPTG and then harvested by centrifugation for 30 min at 4000*g* at 4 °C. $McpR_{His}$ induction was verified by 12% tricine–SDS-PAGE, followed by Coomassie Blue staining and by Western blot using an anti-His antibody (MBL; PM032). To purify $McpR_{His}$, the IPTG-induced culture was washed with binding buffer (20 mM Tris–HCl (pH 8.0), 500 mM NaCl, 10% glycerol, and 10 mM $MgCl_2$) supplemented with 400 mg lysozyme (Sigma), complete EDTA-free protease cocktail inhibitor (Roche), 5 mg DNase I (Roche), and 0.4 g SDS and centrifuged for 15 min at 9000*g* at 4 °C. Bacterial cells were lysed at 2.4 kbar using a Cell disruptor (Cell Disruption System—one shot model, Constant). As $McpR_{His}$ was mainly forming inclusion bodies, the pellet fraction was resuspended for 1 h under shaking at 4 °C in the binding buffer containing 6 M guanidine. The solubilized inclusion bodies were centrifuged for 30 min at 9000*g* at 4 °C. The collected supernatant was dialyzed overnight in a 0.1 M phosphate buffer (12.5 mM Na_2HPO_4, 8 mM KH_2PO_4, pH 8) to remove guanidine, allowing the refolding of McpR. The same methodology was applied for the C75S and H99A mutants.

McpR protein concentration was determined (i) by measuring the absorbance of the sample at 280 nm with the SpectraMax iD3 or (ii) with a Bradford protein assay.

Fluorescence quenching by Cu and other metal ions

Purified McpR at a concentration of 3.58 μM was incubated with different ratios of $CuSO_4$, *Tetrakis*(*acetonitrile*)*Cu*(I) *hexafluorophosphate*, $ZnSO_4$, $CdSO_4$, $MnSO_4$, and $NiSO_4$ in black bottom 96-well plates. The fluorescence emission spectra were recorded upon 280 nm excitation with the SpectraMax iD3.

K_d determination

The titration of McpR by Cu(I) or Cu(II) monitored by the protein intrinsic fluorescence intensity quenching was fitted to a single-site hyperbolic model by nonlinear regression using the SciDAVis 2.7 software (https://scidavis.sourceforge.net/index.html) to determine the affinity constants, according to the following equation:

Fluorescence intensity = F0 + A*[Cu]/(K_d + [Cu]), with F0 corresponding to the fluorescence intensity of the apo McpR, A to the total fluorescence amplitude change upon Cu binding and K_d to the affinity dissociation constant. Dissociation constants are reported as the mean value ± SD obtained for a minimum of two independent experiments performed on distinct protein productions.

Identification of McpR oxidation by mass spectrometry

Sample preparation and protein digestion

About 15 μg of purified McpR or $McpR_{C75S}$ were incubated with Cu(II), Cu(I), H_2O_2, and Cu(I) + H_2O_2 at a 1:100 ratio for 10 min at room temperature. McpR samples were treated using filter-aided sample preparation using the following protocol. To first wash the filter, 100 μl of 1% formic acid were placed in each Millipore Microcon 30 MRCFOR030 Ultracel PL-30 before a 15 min centrifugation at 14,100*g*. For each sample, 40 μg of protein adjusted in 150 μl of 8 M urea buffer (8 M urea in 0.1 M Tris buffer at pH 8.5) were placed individually in a column and centrifuged for 15 min at 14,100*g*. The filtrate was discarded, and the columns were washed three times by adding 200 μl of urea buffer followed by a 15 min centrifugation at 14,100*g*. For the reduction step, 100 μl of DTT were added and mixed for 1 min at 400 rpm with a thermomixer before a 15 min incubation at 24 °C. The samples were then centrifugated for 15 min at 14,100*g*, the filtrate was discarded, and the filter was washed by adding 100 μl of urea buffer before another 15 min centrifugation at 14,100*g*. An alkylation step was performed by adding 100 μl of iodoacetamide ([IAA], in urea buffer) in the column and mixing for 1 min at 400 rpm in the dark followed by a 20 min incubation in the dark and a 10 min centrifugation at 14,100*g*. To remove the excess of IAA, 100 μl of urea buffer were added and the samples were centrifuged for 15 min at 14,100*g*. To quench the rest of IAA, 100 μl of DTT were placed on the column, mixed for 1 min at 400 rpm, and incubated for 15 min at 24 °C before a 10 min centrifugation at 14,100*g*. To remove the excess of DTT, 100 μl of urea buffer were placed on the column and centrifuged for 15 min at 14,100*g*. The filtrate was discarded, and the column was washed three times by adding 100 μl of 50 mM sodium bicarbonate buffer ([ABC], in ultrapure water) followed by a 10 min centrifugation at 14,100*g*. The remaining 100 μl were kept at the bottom of the column to avoid any evaporation in the column. The digestion process was performed by adding 80 μl of mass spectrometry (MS) grade trypsin (1/50 in ABC buffer) in the column and mixed for 1 min at 400 rpm followed by an overnight incubation at 24 °C in a water saturated environment. The Microcon columns were placed in a 1.5 ml LoBind tube and centrifuged for 10 min at 14,100*g*. Forty microliters of ABC buffer were placed on the column before a 10 min centrifugation at 14,100*g*. Ten percent of TFA in ultrapure water were added into the LoBind Tube to obtain 0.2% TFA. The samples were dried in a SpeedVac up to 20 μl and transferred into an injection vial.

MS

The digest was analyzed using nano-LC–ESI–MS/MS timsTOF Pro (Bruker) coupled with an UHPLC nanoElute (Bruker).

Peptides were separated by nanoUHPLC (nanoElute; Bruker) on a 75 μm ID, 25 cm C18 column with integrated CaptiveSpray insert (Aurora, IonOpticks) at a flow rate of 400 nl/min, at 50 °C. LC mobile phase A was water with 0.1% formic acid (v/v) and B acetonitrile with 0.1% formic acid (v/v). Samples were loaded directly on the analytical column at a constant pressure of 800 bar. The digest (1 μl) was injected, and the organic content of the mobile phase was increased linearly from 2% B to 15% in 36 min, from 15% B to 25% in 19 min, from 25% B to 37% in 5 min, and from 37% B to 95% in 5 min. Data acquisition on the timsTOF Pro was performed

using Hystar 5.1 and timsControl 2.0. timsTOF Pro (Bruker) data were acquired using 100 ms TIMS accumulation time, mobility (1/K0) range from 0.6 to 1.6 Vs/cm^2. Mass spectrometric analysis was carried out using the parallel accumulation serial fragmentation acquisition method. One MS spectra followed by ten parallel accumulation serial fragmentation MSMS spectra per total cycle of 1.1 s.

Data analysis was performed using PEAKS Studio X Pro with ion mobility module (Bioinformatics Solutions, Inc). Protein identifications were conducted using PEAKS search engine with 15 ppm as parent mass error tolerance and 0.05 Da as fragment mass error tolerance. Carbamidomethylation was allowed as fixed modification, oxidation of methionine, histidine, tryptophan, and acetylation (N-term) as variable modification. Enzyme specificity was set to trypsin, and the maximum number of missed cleavages per peptide was set at 3. The peak lists were searched against the *E. coli*-K12 (11,002 sequences) and *Caulobacter* NA1000 (3863 sequences) from UNIREF 100. Peptide spectrum matches and protein identifications were normalized to less than 1.0% false discovery rate.

The identification results were processed with the PTM profile tool from PEAKS, which provides quantitative information of modified peptides compared with unmodified peptides for the modification sites of the protein across all MS samples (49, 50).

The MS proteomics data have been deposited to the ProteomeXchange Consortium *via* the PRIDE (51) partner repository with the dataset identifier PXD044512 and 10.6019/PXD044512.

CD

Purified McpR at a concentration of 8.95 μM was incubated with different $CuSO_4$ and *Tetrakis*(*acetonitrile*)*Cu*(I) *hexafluorophosphate* concentrations. Measurements were performed with an MOS-500 spectropolarimeter in the far-UV region (190–260 nm), using a 1 mm pathlength cell. Four scans were averaged, and base lines were subtracted. Secondary structure analyses were performed on the CD data with the BeStSel server.

Data availability

All data are contained within the article and supporting information section. The raw data can be shared upon request to jean-yves.matroule@unamur.be.

Supporting information—This article contains supporting information (16, 17, 52–54).

Acknowledgments—We thank Jakob R. Winther for providing the rxYFP construct. We are also grateful to Valérie Charles and Carmela Aprile (CMI laboratory, NISM, UNamur) for the ICP measurements and to Virgile Neyman for technical support during the protein purification. Finally, we acknowledge Jean-François Collet and Xavier De Bolle for critical reading of this article and the URBM members and Johan Wouters (Chemistry Department, UNamur) for fruitful discussions.

Author contributions—G. L. and J.-Y. M. conceptualization; G. L. methodology; G. L. validation; G. L., P. C., C. M., S. R.-C., M. D., R. V. H., P. R., E. P., and J.-Y. M. formal analysis; G. L., P. C., C. M., M. D., F. T., L. M., and E. P. investigation; G. L. writing–original draft; G. L. visualization; J.-Y. M. writing–review & editing; J.-Y. M. supervision; J-.Y. M. funding acquisition.

Funding and additional information—This work was supported by the University of Namur. G. L. was supported by the Belgian Fund for Industrial and Agricultural Research Associate (FRIA/FNRS). Catherine Michaux and Eric Perpète thank the Belgian National Fund for Scientific Research (FNRS) for their respective associate and senior research associate positions.

Conflict of interest—The authors declare that they have no conflicts of interest with the contents of this article.

Abbreviations—The abbreviations used are: ABC, sodium bicarbonate buffer; Cd, cadmium; Cu, copper; H_2O_2, hydrogen peroxide; IAA, iodoacetamide; ICP-OES, inductively coupled plasma optical emission spectrometry; LCI, live chemotaxis imaging; MCP, methyl-accepting chemotaxis protein; MS, mass spectrometry; PDMS, polydimethylsiloxane; PYE, peptone yeast extract; ROS, reactive oxygen species; SW, swarmer cell; TM, transmembrane domain; Zn, zinc.

References

1. Wadhams, G. H., and Armitage, J. P. (2004) Making sense of it all: bacterial chemotaxis. *Nat. Rev. Mol. Cell Biol.* **5**, 1024–1037
2. Thomas, M. A., Kleist, A. B., and Volkman, B. F. (2018) Decoding the chemotactic signal. *J. Leukoc. Biol.* **104**, 359–374
3. Silversmith, R. E. (2010) Auxiliary phosphatases in two-component signal transduction. *Curr. Opin. Microbiol.* **13**, 177–183
4. Sircar, R., Greenswag, A. R., Bilwes, A. M., Gonzalez-Bonet, G., and Crane, B. R. (2013) Structure and activity of the flagellar rotor protein FliY: a member of the CheC phosphatase family. *J. Biol. Chem.* **288**, 13493–13502
5. Lertsethtakarn, P., Howitt, M. R., Castellon, J., Amieva, M. R., and Ottemann, K. M. (2015) Helicobacter pylori CheZ(HP) and ChePep form a novel chemotaxis-regulatory complex distinct from the core chemotaxis signaling proteins and the flagellar motor. *Mol. Microbiol.* **97**, 1063–1078
6. Briegel, A., Wong, M. L., Hodges, H. L., Oikonomou, C. M., Piasta, K. N., Harris, M. J., *et al.* (2014) New insights into bacterial chemoreceptor array structure and assembly from electron cryotomography. *Biochemistry* **53**, 1575–1585
7. Samanta, D., Borbat, P. P., Dzikovski, B., Freed, J. H., and Crane, B. R. (2015) Bacterial chemoreceptor dynamics correlate with activity state and are coupled over long distances. *Proc. Natl. Acad. Sci. U. S. A.* **112**, 2455–2460
8. Flack, C. E., and Parkinson, J. S. (2022) Structural signatures of Escherichia coli chemoreceptor signaling states revealed by cellular crosslinking. *Proc. Natl. Acad. Sci. U. S. A.* **119**, e2204161119
9. Parkinson, J. S., Hazelbauer, G. L., and Falke, J. J. (2015) Signaling and sensory adaptation in Escherichia coli chemoreceptors: 2015 update. *Trends Microbiol.* **23**, 257–266
10. Macomber, L., and Imlay, J. A. (2009) The iron-sulfur clusters of dehydratases are primary intracellular targets of copper toxicity. *Proc. Natl. Acad. Sci. U. S. A.* **106**, 8344–8349
11. Giachino, A., and Waldron, K. J. (2020) Copper tolerance in bacteria requires the activation of multiple accessory pathways. *Mol. Microbiol.* **114**, 377–390
12. Lawaree, E., Gillet, S., Louis, G., Tilquin, F., Le Blastier, S., Cambier, P., *et al.* (2016) Caulobacter crescentus intrinsic dimorphism

provides a prompt bimodal response to copper stress. *Nat. Microbiol.* **1**, 16098
13. Kovarik, M. L., Brown, P. J., Kysela, D. T., Berne, C., Kinsella, A. C., Brun, Y. V., *et al.* (2010) Microchannel-nanopore device for bacterial chemotaxis assays. *Anal. Chem.* **82**, 9357–9364
14. Morse, M., Colin, R., Wilson, L. G., and Tang, J. X. (2016) The aerotactic response of Caulobacter crescentus. *Biophys. J.* **110**, 2076–2084
15. Nesper, J., Hug, I., Kato, S., Hee, C. S., Habazettl, J. M., Manfredi, P., *et al.* (2017) Cyclic di-GMP differentially tunes a bacterial flagellar motor through a novel class of CheY-like regulators. *Elife* **6**, e28842
16. Berne, C., and Brun, Y. V. (2019) The two chemotaxis clusters in Caulobacter crescentus play different roles in chemotaxis and biofilm regulation. *J. Bacteriol.* **201**, e00071-19
17. Tsai, J. W., and Alley, M. R. (2000) Proteolysis of the McpA chemoreceptor does not require the Caulobacter major chemotaxis operon. *J. Bacteriol.* **182**, 504–507
18. Sourjik, V., and Schmitt, R. (1998) Phosphotransfer between CheA, CheY1, and CheY2 in the chemotaxis signal transduction chain of Rhizobium meliloti. *Biochemistry* **37**, 2327–2335
19. Briegel, A., Ding, H. J., Li, Z., Werner, J., Gitai, Z., Dias, D. P., *et al.* (2008) Location and architecture of the Caulobacter crescentus chemoreceptor array. *Mol. Microbiol.* **69**, 30–41
20. Potocka, I., Thein, M., Østerås, M., Jenal, U., and Alley, M. R. (2002) Degradation of a Caulobacter soluble cytoplasmic chemoreceptor is ClpX dependent. *J. Bacteriol.* **184**, 6635–6641
21. Nierman, W. C., Feldblyum, T. V., Laub, M. T., Paulsen, I. T., Nelson, K. E., Eisen, J. A., *et al.* (2001) Complete genome sequence of Caulobacter crescentus. *Proc. Natl. Acad. Sci. U. S. A.* **98**, 4136–4141
22. Lamb, A. L., Wernimont, A. K., Pufahl, R. A., Culotta, V. C., O'Halloran, T. V., and Rosenzweig, A. C. (1999) Crystal structure of the copper chaperone for superoxide dismutase. *Nat. Struct. Biol.* **6**, 724–729
23. Drozdetskiy, A., Cole, C., Procter, J., and Barton, G. J. (2015) JPred4: a protein secondary structure prediction server. *Nucleic Acids Res.* **43**, W389–W394
24. Barnakov, A. N., Barnakova, L. A., and Hazelbauer, G. L. (1998) Comparison *in vitro* of a high- and a low-abundance chemoreceptor of Escherichia coli: similar kinase activation but different methyl-accepting activities. *J. Bacteriol.* **180**, 6713–6718
25. Krogh, A., Larsson, B., von Heijne, G., and Sonnhammer, E. L. (2001) Predicting transmembrane protein topology with a Hidden Markov model: application to complete genomes. *J. Mol. Biol.* **305**, 567–580
26. Teufel, F., Almagro Armenteros, J. J., Johansen, A. R., Gislason, M. H., Pihl, S. I., Tsirigos, K. D., *et al.* (2022) SignalP 6.0 predicts all five types of signal peptides using protein language models. *Nat. Biotechnol.* **40**, 1023–1025
27. Neumann, S., Hansen, C. H., Wingreen, N. S., and Sourjik, V. (2010) Differences in signalling by directly and indirectly binding ligands in bacterial chemotaxis. *EMBO J.* **29**, 3484–3495
28. Jumper, J., Evans, R., Pritzel, A., Green, T., Figurnov, M., Ronneberger, O., *et al.* (2021) Highly accurate protein structure prediction with AlphaFold. *Nature* **596**, 583–589
29. Varadi, M., Anyango, S., Deshpande, M., Nair, S., Natassia, C., Yordanova, G., *et al.* (2022) AlphaFold protein structure database: massively expanding the structural coverage of protein-sequence space with high-accuracy models. *Nucleic Acids Res.* **50**, D439–D444
30. Rubino, J. T., and Franz, K. J. (2012) Coordination chemistry of copper proteins: how nature handles a toxic cargo for essential function. *J. Inorg. Biochem.* **107**, 129–143
31. Xiao, Z., Brose, J., Schimo, S., Ackland, S. M., La Fontaine, S., and Wedd, A. G. (2011) Unification of the copper(I) binding affinities of the metallochaperones Atx1, Atox1, and related proteins: detection probes and affinity standards. *J. Biol. Chem.* **286**, 11047–11055
32. Kahra, D., Kovermann, M., and Wittung-Stafshede, P. (2016) The C-terminus of human copper importer Ctr1 acts as a binding site and transfers copper to Atox1. *Biophys. J.* **110**, 95–102
33. Maertens, L., Cherry, P., Tilquin, F., Van Houdt, R., and Matroule, J. Y. (2021) Environmental conditions modulate the transcriptomic response of both Caulobacter crescentus morphotypes to Cu stress. *Microorganisms* **9**, 1116
34. Lee, J. W., and Helmann, J. D. (2006) The PerR transcription factor senses H2O2 by metal-catalysed histidine oxidation. *Nature* **440**, 363–367
35. Tiwari, M. K., Hagglund, P. M., Moller, I. M., Davies, M. J., and Bjerrum, M. J. (2019) Copper ion/H2O2 oxidation of Cu/Zn-superoxide dismutase: implications for enzymatic activity and antioxidant action. *Redox Biol.* **26**, 101262
36. Ramteke, S. N., Walke, G. R., Joshi, B. N., Rapole, S., and Kulkarni, P. P. (2014) Effects of oxidation on redox and cytotoxic properties of copper complex of Abeta1-16 peptide. *Free Radic. Res.* **48**, 1417–1425
37. Stadtman, E. R. (1993) Oxidation of free amino acids and amino acid residues in proteins by radiolysis and by metal-catalyzed reactions. *Annu. Rev. Biochem.* **62**, 797–821
38. Rubino, J. T., Chenkin, M. P., Keller, M., Riggs-Gelasco, P., and Franz, K. J. (2011) A comparison of methionine, histidine and cysteine in copper(I)-binding peptides reveals differences relevant to copper uptake by organisms in diverse environments. *Metallomics* **3**, 61–73
39. Chervitz, S. A., and Falke, J. J. (1996) Molecular mechanism of transmembrane signaling by the aspartate receptor: a model. *Proc. Natl. Acad. Sci. U. S. A.* **93**, 2545–2550
40. Salah Ud-Din, A. I. M., and Roujeinikova, A. (2017) Methyl-accepting chemotaxis proteins: a core sensing element in prokaryotes and archaea. *Cell. Mol. Life Sci.* **74**, 3293–3303
41. Dupont, C. L., Grass, G., and Rensing, C. (2011) Copper toxicity and the origin of bacterial resistance–new insights and applications. *Metallomics* **3**, 1109–1118
42. Macomber, L., Rensing, C., and Imlay, J. A. (2007) Intracellular copper does not catalyze the formation of oxidative DNA damage in Escherichia coli. *J. Bacteriol.* **189**, 1616–1626
43. Khursigara, C. M., Wu, X., and Subramaniam, S. (2008) Chemoreceptors in Caulobacter crescentus: trimers of receptor dimers in a partially ordered hexagonally packed array. *J. Bacteriol.* **190**, 6805–6810
44. Webre, D. J., Wolanin, P. M., and Stock, J. B. (2003) Bacterial chemotaxis. *Curr. Biol.* **13**, R47–R49
45. Poindexter, J. S. (1981) The caulobacters: ubiquitous unusual bacteria. *Microbiol. Rev.* **45**, 123–179
46. Evinger, M., and Agabian, N. (1977) Envelope-associated nucleoid from Caulobacter crescentus stalked and swarmer cells. *J. Bacteriol.* **132**, 294–301
47. Ostergaard, H., Tachibana, C., and Winther, J. R. (2004) Monitoring disulfide bond formation in the eukaryotic cytosol. *J. Cell Biol.* **166**, 337–345
48. Ducret, A., Quardokus, E. M., and Brun, Y. V. (2016) MicrobeJ, a tool for high throughput bacterial cell detection and quantitative analysis. *Nat. Microbiol.* **1**, 16077
49. Meier, F., Brunner, A. D., Koch, S., Koch, H., Lubeck, M., Krause, M., *et al.* (2018) Online parallel accumulation-serial fragmentation (PASEF) with a novel trapped ion mobility mass spectrometer. *Mol. Cell. Proteomics* **17**, 2534–2545
50. Zhang, J., Xin, L., Shan, B., Chen, W., Xie, M., Yuen, D., *et al.* (2012) PEAKS DB: de novo sequencing assisted database search for sensitive and accurate peptide identification. *Mol. Cell. Proteomics* **11**. M111. 010587
51. Perez-Riverol, Y., Bai, J., Bandla, C., Garcia-Seisdedos, D., Hewapathirana, S., Kamatchinathan, S., *et al.* (2022) The PRIDE database resources in 2022: a hub for mass spectrometry-based proteomics evidences. *Nucleic Acids Res.* **50**, D543–D552
52. Alley, M. R., Maddock, J. R., and Shapiro, L. (1992) Polar localization of a bacterial chemoreceptor. *Genes Dev* **6**, 825–836
53. Alley, M. R., Maddock, J. R., and Shapiro, L. (1993) Requirement of the carboxyl terminus of a bacterial chemoreceptor for its targeted proteolysis. *Science* **259**, 1754–1757
54. Tsai, J. W., and Alley, M. R. (2001) Proteolysis of the Caulobacter McpA chemoreceptor is cell cycle regulated by a ClpX-dependent pathway. *J Bacteriol* **183**, 5001–5007